



Technical Note

Mapping Soil Organic Matter Using Different Modeling Techniques in the Dryland Agroecosystem of Huang-Huai-Hai Plain, Eastern China

Hua Jin ¹, Xuefeng Xie ^{1,*} , Lijie Pu ^{2,3}, Zhenyi Jia ¹ and Fei Xu ⁴

¹ College of Geography and Environmental Sciences, Zhejiang Normal University, Jinhua 321004, China; zhenyijay@zjnu.edu.cn (Z.J.)

² School of Environmental Engineering, Nanjing Institute of Technology, Nanjing 211167, China

³ School of Geography and Ocean Science, Nanjing University, Nanjing 210023, China

⁴ Institute of Land and Urban-Rural Development, Zhejiang University of Finance & Economics, Hangzhou 310018, China; xufei16@zufe.edu.cn

* Correspondence: xiexuefeng@zjnu.cn

Abstract: Accurately mapping the spatial distribution and variation of soil organic matter (SOM) is of great significance for guiding regional soil management. However, the applicability and prediction performance of machine learning techniques in dryland agroecosystems still needs to be further studied. In this study, we collected a total of 733 topsoil samples from the farmland in Xiao County, Anhui Province, which is a typical dryland agroecosystem in the Huang-Huai-Hai Plain. Then, the environmental covariates were selected, and the ordinary kriging (OK), multiple linear stepwise regression (MLR), regression kriging (RK), radial basis function neural network (RBFNN), and random forest (RF) models were conducted to map the SOM content, and the optimal model was ascertained. The results demonstrated that the alkali-hydrolyzable nitrogen (26.11%), available potassium (17.73%), mean annual precipitation (13.26%), and pH (11.80%) were the main controlling factors affecting the spatial distribution of SOM in the study area. Meanwhile, the introduction of environmental covariates can effectively improve the SOM prediction accuracy, and the RF model ($R^2 = 0.48$, MAE = 2.38 g kg⁻¹, MRE = 12.99%, RMSE = 3.14 g kg⁻¹) has a better performance than the RBFNN, MLR, RK, and OK methods. Although there are local differences in the spatial distribution of SOM predicted by the five methods, the overall spatial distribution of SOM was characterized by the low concentration area (13.44–20.00 g kg⁻¹) distributed in the central and northwest of study area, and the high concentration area (24.00–28.95 g kg⁻¹) distributed in the southeast. Overall, our study demonstrated that machine learning-based models could accurately predict the SOM content in dryland agroecosystem, and the produced maps function as baseline maps for sustainable agricultural management.

Keywords: soil organic matter; digital soil mapping; random forest; main control factors; fluvisols



Citation: Jin, H.; Xie, X.; Pu, L.; Jia, Z.; Xu, F. Mapping Soil Organic Matter Using Different Modeling Techniques in the Dryland Agroecosystem of Huang-Huai-Hai Plain, Eastern China. *Remote Sens.* **2023**, *15*, 4945. <https://doi.org/10.3390/rs15204945>

Academic Editor: Jeroen Meersmans

Received: 7 September 2023

Revised: 6 October 2023

Accepted: 11 October 2023

Published: 13 October 2023



Copyright: © 2023 by the authors. Licensee MDPI, Basel, Switzerland. This article is an open access article distributed under the terms and conditions of the Creative Commons Attribution (CC BY) license (<https://creativecommons.org/licenses/by/4.0/>).

1. Introduction

Soil organic matter (SOM) is an important component of soil and the basis of soil fertility [1–3]. SOM is considered to be the key attribute affecting soil function and ecosystem services and plays a vital role in the material cycle of the terrestrial ecosystem [4–6]. Hence, exploring the spatial distribution of SOM is the starting-point of realizing soil sustainable utilization. However, the content of SOM in farmland is affected by complex natural (climate, topography, parent soil material, etc.) and anthropogenic (fertilization, rotation system, etc.) factors, showing an uneven spatial distribution, which directly affects the soil quality and crop yield in an agroecosystem [7–9]. Therefore, obtaining high-precision spatial distribution of SOM in farmland is the key to improving agricultural productivity and is still a challenging task.

Digital soil mapping (DSM) quantitatively analyzes the relationship between soil attributes and the surrounding environment through neighborhood analysis and mathematical modeling methods and predicts the spatial distribution pattern of the soil–landscape continuum [10,11], which can reduce the cost of sampling and analysis to a certain extent and has been widely recognized and applied [11–13]. At present, three main types of quantitative methods were used in DSM: (i) geostatistical models that do not consider deterministic trends, such as ordinary kriging (OK) [14,15]; (ii) identifying the random spatial correlation changes and employing a mixed method to determine the trend, such as regression kriging (RK) [16,17]; and (iii) machine learning models based on feature space who do not explicitly consider the relevant changes in random space; for example, radial basis function neural network (RBFNN), support vector machine (SVM), and random forest (RF) [18–20]. Soil is a spatiotemporal continuum with high variability, and the effect of soil-forming factors on soil is nonlinear during the formation and development of soil [21]. Therefore, traditional global models, such as multiple linear regression (MLR) and OK, cannot fit the nonlinear relationship between environmental factors and soil properties at the regional scale [22]. Machine learning algorithms have excellent applicability in processing multidimensional and nonlinear massive data, improving model generalization ability, and are therefore applied in the spatial prediction of soil attributes and have been proven to effectively improve the prediction accuracy compared with linear regression models due to their strong self-adaptability [19,23]. Although these models have achieved merit application results, they also have some defects, such as an unstable modeling process, and sometimes the results are difficult to explain and run the risk of overfitting [24,25]. These models cannot quantify and rank the contribution of environmental factors affecting the spatial distribution of soil attributes, which presents certain limitations in their use [22]. The RF model has strong nonlinear mining ability, resistance to overfitting, and the advantage of explaining complex multivariable under few parameters' adjustment, which is more suitable for simulating soil properties with strong high-order interaction [12,26,27]. Compared with other nonlinear regression models, random forest can quantify and rank the importance of different environmental variables, so it is widely introduced into the prediction of soil attributes [24,28].

Although there is no lack of comparative research on DSM application models for SOM prediction, the applicability and prediction performance of these models in dryland agroecosystems still need to be further studied. Therefore, we hypothesize that the machine learning-based models have higher prediction accuracy in predicting the SOM content in dryland agroecosystems. Consequently, the specific objectives of this study were to (i) evaluate the performance of nonlinear models (i.e., RF, RBFNN) and linear models (i.e., OK, MLR, RK) in predicting SOM using multisource environmental covariates; and (ii) identify the most influential environmental covariates controlling the variation of SOM in a dryland agroecosystem. This study will provide a scientific basis for SOM prediction and land use planning and decision making in a dryland agroecosystem.

2. Materials and Methods

2.1. Study Area

Xiao County covers 1885 km² and is located in the north of Anhui Province and the southern part of Huang-Huai-Hai Plain (33°56'21"–34°29'27"N, 116°31'23"–117°8'46"E) (Figure 1). This region belongs to the warm temperate monsoon climate zone, with an annual average temperature of 14.3 °C and an annual average precipitation of 854.6 mm. The terrain of the whole area is slightly inclined from northwest to southeast, with an altitude of –31–385 m, which is divided into low mountains and hills and Yellow River floodplains, accounting for 22.2% and 77.8% of the total area, respectively. The soil originated from the alluvial deposits of the Yellow River, with a sandy loam texture. Farmland, orchard, forest land, and construction land are the main patterns of land use in the county, accounting for 60.6%, 6.2%, 5.4%, and 15.7% of the total area, respectively. More specifically, the dryland

cropping area accounts for 89.4% of the total farmland area. The dryland crops include wheat (*Triticum aestivum* L.), corn (*Zea mays* Linn.), and soybean (*Glycine max*).

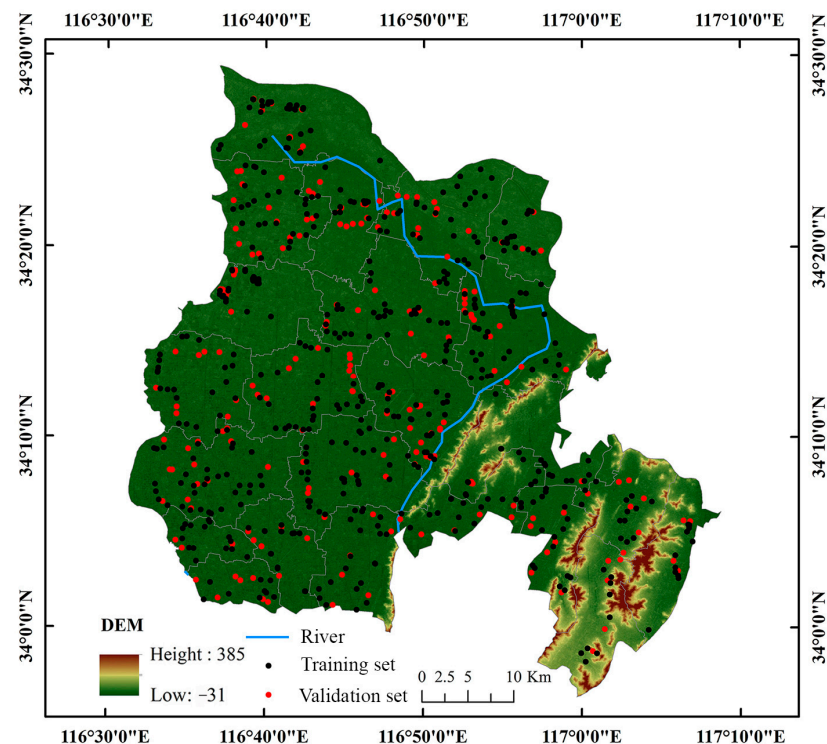


Figure 1. Location of the study area and sampling sites.

2.2. Data Sources and Processing

2.2.1. Soil Collection and Analysis

From July to August 2015, field sampling points were arranged on the farmland of the whole region, and soil samples were collected from a depth of 0–20 cm of the cultivated horizon using a stainless steel corer. More specifically, five subsamples within a 5 m radius were collected and uniformly mixed to form a composite sample at each sample site, and a total of 733 soil samples were collected. The longitude and latitude of the sampling points are recorded with GPS. SOM concentration was determined via the method of oxidation with $K_2Cr_2O_7$ in a heated oil bath; pH value was determined via the pH meter; alkali-hydrolysable nitrogen was determined via Kjaerd method; available phosphorus was determined via spectrophotometry; and available potassium was determined via a flame photometer [29].

2.2.2. Sources of Auxiliary Variables

In this study, the terrain, climate, vegetation, primary productivity, spectral, and soil attribute indexes were selected as environmental covariates to predict the spatial distribution of SOM. All environmental covariates were acquired in 2015 except for terrain indexes, and the specific composition of environmental covariates is shown in Table 1. The annual average precipitation and annual average temperature are selected from the spatial interpolation dataset of annual precipitation in China and the spatial interpolation dataset of annual average temperature in China from the Resource and Environmental Sciences and Data Center, Chinese Academy of Sciences (<http://www.resdc.cn/> (accessed on 14 March 2021)). The vegetation index and spectral index were obtained by computing Landsat 8 OLI_TIRS images from the Geospatial Data Cloud Platform of the Chinese Academy of Sciences (<http://www.gscloud.cn/> (accessed on 14 March 2021)). The terrain index data were obtained from global digital elevation data (ASTER GDEM V2) of the Geospatial Data Cloud Platform, Chinese Academy of Sciences (<http://www.gscloud.cn/>

(accessed on 14 March 2021)). The net primary productivity (NPP) was obtained from a monthly 1 km raster dataset of net primary productivity of terrestrial ecosystems in China north of 18°N (1985–2015), published by The Global Change Science Data Publishing System (<http://www.geodoi.ac.cn/> (accessed on 14 March 2021)). For the environmental covariates with low spatial resolution, such as mean annual precipitation (MAP), mean annual temperature (MAT), and net primary productivity (NPP), the nearest neighbor method was used to reduce the spatial scale to 30 m × 30 m for SOM spatial prediction. For soil attributes, such as soil pH, AN, AP, and AK, the ordinary kriging method was used for interpolation, and the interpolated grid data (30 m × 30 m) was used as the auxiliary factor of SOM spatial prediction.

Table 1. Composition of auxiliary variables.

Types	Auxiliary Variables	References
Terrain	elevation, slope, aspect, relief degree of land surface (RDLs), surface roughness (SR), surface cutting depth (SCD), topographic wetness index (TWI), stream power index (SPI), sediment transport index (STI)	[17,30–32]
Climate	mean annual precipitation (MAP), mean annual temperature (MAT)	[33,34]
Vegetation	ratio vegetation index (RVI), normalized difference vegetation index (NDVI), difference vegetation index (DVI)	[31,35,36]
Primary productivity	net primary productivity (NPP)	[37]
Spectral	blue (Band 2), green (Band 3), red (Band 4), near infrared (Band 5), short-wavelength infrared 1 (Band 6), short-wavelength infrared 2 (Band 7), ratio of band	[38–40]
Soil attributes	pH, alkali-hydrolyzable nitrogen (AN), available phosphorus (AP), available potassium (AK)	[25,41]

2.3. Model Development and Validation

Ordinary kriging (OK) is a commonly used spatial interpolation method. Assuming that the average value of regional variables is an unknown constant in the whole study area, the weighting factor is determined by the semi-variogram based on unbiased prediction and minimum variance [15,42]. The OK model requires the normal distribution of the original data or the data after function transformation before calculation.

The multiple linear regression (MLR) model assumes that the relationship between soil attributes and environmental covariates is linear and makes predictions by constructing the approximate expression between the soil attributes and multiple environmental covariates [22,36]. The multiple stepwise regression tries to introduce variables one by one, and each new variable will test the significance of the introduced variables, eliminate the insignificant environmental covariates, and use the final retained variables and soil attributes to construct a linear regression equation [27,43].

The regression kriging (RK) model is an extension of the OK model, and its observations are regarded as the sum of drift and residual [44,45]. RK first uses MLR to predict the soil attributes based on the auxiliary predictors retained via stepwise regression analysis, then makes an OK prediction for the residual of soil attributes predicted via MLR, and finally adds the regression prediction value and the OK prediction value of the residual to obtain the prediction value of soil attributes [16,17].

The radial basis function neural network model (RBFNN) is a three-layer feedforward neural network model with a single hidden layer [31,46]. It can approach any continuous function with any accuracy and combine network and fuzzy logic so as to improve the

generalization ability of the algorithm [36]. RBFNN has the characteristics of parallel computing, distributed storage, strong fault tolerance, and fast learning, which have obvious advantages in learning speed and parameter setting compared with the BP neural network model [19,47].

Random forest (RF) is a data mining algorithm based on multiple decision trees [26,27,48]. By using the bootstrap method to randomly select samples in the training data set to build a separate tree model, a large number of trees are generated to form a random forest [12,28]. Compared with the cart decision tree model, the RF model is sensitive to overfitting, which can not only better deal with the complex nonlinear relationship between variables but also overcome the defects of overfitting and complex calculation [22,24].

In the model development, 70% of soil samples (514 samples) were randomly selected as the training set to participate in the modeling, and the remaining 30% of samples (219 samples) were selected as the validation set to verify the interpolation accuracy. The performance of the prediction models was evaluated using a 10-fold cross-validation procedure that involved comparisons between the predicted and observed SOM values, and four validation measurements were calculated, i.e., coefficient of determination (R^2), mean absolute error (MAE), mean relative error (MRE), and root mean square error (RMSE), defined as follows:

$$R^2 = \frac{\sum_{i=1}^n (P_i - \bar{O}_i)^2}{\sum_{i=1}^n (O_i - \bar{O}_i)^2}, \quad (1)$$

$$\text{MAE} = \frac{1}{n} \sum_{i=1}^n |P_i - O_i|, \quad (2)$$

$$\text{MRE} = \frac{1}{n} \sum_{i=1}^n \frac{|P_i - O_i|}{O_i}, \quad (3)$$

$$\text{RMSE} = \sqrt{\frac{1}{n} \sum_{i=1}^n (O_i - P_i)^2}, \quad (4)$$

where P_i and O_i are the predicted and observed values at site i , respectively; \bar{O}_i is the mean observed values; and n is the number of samples.

2.4. Statistical Analyses

The descriptive statistical analysis and Pearson correlation analysis were completed in SPSS 25. To avoid the influence of multicollinearity of variables on the prediction accuracy of the model, the variance inflation factor (VIF) of all environmental covariates is calculated, and the variables with VIF > 10 are removed. The spatial data processing and mapping were carried out in ArcGIS 10.3, and the relative importance and response curve of each environmental covariate to SOM were derived from the RF model.

3. Results

3.1. Descriptive Statistics

Descriptive statistics show that the SOM contents of the training set and validation set have high similarity (Table 2). The content of SOM in the study area ranged from 7.20 to 32.10 g kg⁻¹, and the average content of SOM in the training set and validation set was 19.56 g kg⁻¹ and 19.51 g kg⁻¹, respectively. According to the nutrient classification criteria of the Second National Soil Survey of China [49], the average content of SOM in the study area was in grade IV (10–20 g kg⁻¹). The standard deviation of the training set and validation set were 4.36 g kg⁻¹ and 4.34 g kg⁻¹, respectively, and the coefficient of variation were 22.29% and 22.25%, respectively. These results indicated that SOM content had a certain degree of variability within the study area.

Table 2. Descriptive statistics of SOM in the training and validation datasets.

Dataset	Number	Min (g kg ⁻¹)	Max (g kg ⁻¹)	Mean (g kg ⁻¹)	S.D (g kg ⁻¹)	CV (%)
Training	514	7.20	32.10	19.56	4.36	22.29
Validation	219	10.20	31.90	19.51	4.34	22.25

3.2. Relative Importance of Auxiliary Variables

The result of the Pearson correlation analysis shows that there are different degrees of correlation between SOM and other soil attributes in the study area (Table 3). SOM has a significant negative correlation with pH ($r = -0.22$, $p < 0.001$), and a significant positive correlation with AN ($r = 0.59$, $p < 0.001$), AP ($r = 0.15$, $p < 0.001$), and AK ($r = 0.39$, $p < 0.001$). Among the terrain factors, elevation ($r = 0.11$, $p < 0.01$), slope ($r = 0.10$, $p < 0.01$), RDLS ($r = 0.12$, $p < 0.01$), and SCD ($r = 0.12$, $p < 0.01$) were significantly positively correlated with SOM, while SR ($r = 0.09$, $p < 0.05$) was significantly positively correlated with SOM. It should be noted that the retained spectral index was significantly negatively correlated with SOM. MAP was positively correlated with SOM at the significance level of 0.01.

Table 3. Pearson's correlation between SOM and some auxiliary variables.

Auxiliary Variables	Coefficient ¹	Auxiliary Variables	Coefficient
pH	-0.219 ***	RDLS	0.123 **
AN	0.588 ***	SCD	0.119 **
AP	0.153 ***	SR	0.087 *
AK	0.394 ***	Band 2/Band 7	-0.093 *
MAP	0.241 ***	Band 3/Band 6	-0.078 *
Elevation	0.110 **	Band 3/Band 7	-0.100 **
Slope	0.102 **	Band 4/Band 7	-0.092 *

¹ * Significant at 5% probability. ** Significant at 1% probability. *** Significant at 1‰ probability. Variables with significant correlation are listed. AN: alkali-hydrolyzable nitrogen; AK: available potassium; MAP: mean annual precipitation; RDLS: relief degree of land surface; SCD: surface cutting depth; SR: surface roughness.

The relative importance ranking of the environmental covariates derived from the RF model is shown in Table 4. Soil AN and AK are the most important factors affecting the spatial variability of SOM content in the study area, with an explained variation of 26.11% and 17.73%, followed by MAP (13.26%) and pH (11.80%). The increased percentage of the mean square error (% IncMSE) of the first four environmental covariates exceeds 10%, and there is a large gap with the remaining environmental covariates.

Table 4. Variable importance derived from the RF model by the training dataset ($n = 514$) for SOM.

Variables	% IncMSE ¹	Variables	% IncMSE	Variables	% IncMSE
AN	26.11	Band 4/Band 7	6.38	Band 2/Band 7	5.38
AK	17.73	Band 7/Band 6	6.26	Band 2	5.38
MAP	13.26	Band 6/Band 3	6.02	AP	5.32
pH	11.80	Band 4	5.97	Band 5/Band 6	5.27
MAT	8.80	Band 4/Band 3	5.94	Band 3/Band 2	5.23
Band 7/Band 4	7.50	NDVI	5.92	Band 4/Band 5	5.21
Band 6/Band 7	7.02	Band 3	5.79	Band 7/Band 2	5.16
Band 4/Band 6	6.99	Band 2/Band 6	5.73	Band 3/Band 4	5.10
Band 7/Band 5	6.57	Band 2/Band 3	5.60		
Band 7	6.45	Band 6/Band 4	5.49		

¹ Variable importance greater than 5% are listed. AN: alkali-hydrolyzable nitrogen; AK: available potassium; MAP: mean annual precipitation; MAT: mean annual temperature; NDVI: normalized difference vegetation index; AP: available phosphorus.

3.3. Evaluation of Model Performance

As shown in Figure 2, the introduction of environmental covariates can effectively improve the prediction accuracy of SOM. Simultaneously, the prediction accuracy of RBFNN and RF predicted via nonlinear modeling is significantly higher than that of the linear prediction methods (MLR and RK). The R^2 of the predicted results of the validation data has followed the order of RF (0.46) > RBFNN (0.39) > RK (0.21) > MLR (0.20) > OK (0.16), while MAE, MRE, and RMSE are opposite to R^2 , showing RF < RBFNN < RK < MLR < OK. Compared with OK, the MAE, MRE, and RMSE of the RF model decreased by 23.05%, 24.53%, and 20.96%, respectively. This indicated that the RF model has the highest prediction accuracy and can better estimate the spatial distribution of SOM in the study area.

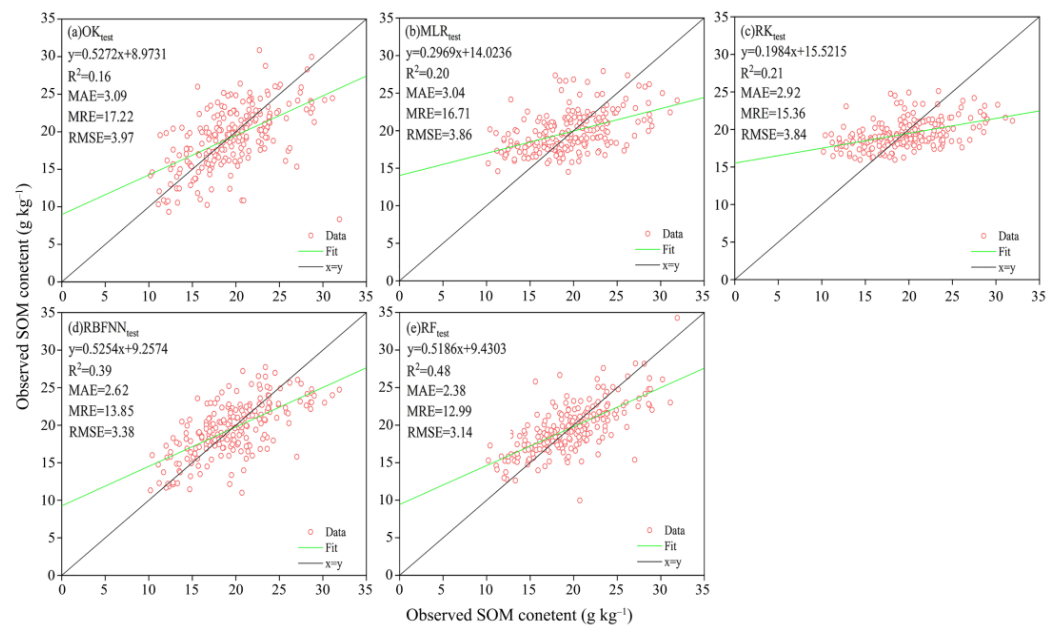


Figure 2. Performance of the OK (a), MLR (b), RK (c), RBFNN (d), and RF (e) models in prediction of SOM.

3.4. Spatial Prediction of SOM

As shown in Figure 3, the spatial distribution of SOM predicted by each model is generally consistent, which is characterized by the fact that the lower center is distributed in the middle area with low terrain ($13.44\text{--}20.00\text{ g kg}^{-1}$), while the higher area is concentrated in the low mountains in the southeast ($24.00\text{--}28.95\text{ g kg}^{-1}$), indicating that the SOM gradually accumulates with the rise of terrain. Compared with OK interpolation, the continuity of SOM spatial distribution predicted by MLR and RK in low- and median-value areas is significantly improved, and the exaggeration and misjudgment in the eastern region is significantly optimized. However, there are also great differences between the MLR and RK in the high value area. MLR has a relatively obvious smoothing effect, resulting in the overestimation of lower values and the underestimation of higher values, which is most prominent in the southeast of the study area. The SOM distribution obtained via RK interpolation is more refined; in particular, the edge transition of the low-value area is more natural, and the fragmentation degree of the middle-value area is effectively reduced, but both show excessively clear boundaries in the high-value area and have a certain degree of distortion. Compared with RK interpolation, the SOM predicted by RBFNN shows more local variation details, but it is characterized by fragmented patches with obvious distribution in both low- and high-value areas. The SOM predicted by RF is closer to the measured value of the sampling points. In the spatial distribution, SOM is characterized by the reduction and connection of the low-value area, the expansion and stability of the median area, and the reduction and concentration of high-value area. The mapping effect

is also more precise, its transition curve is more delicate, and the boundary between high and low values tends to be blurred.

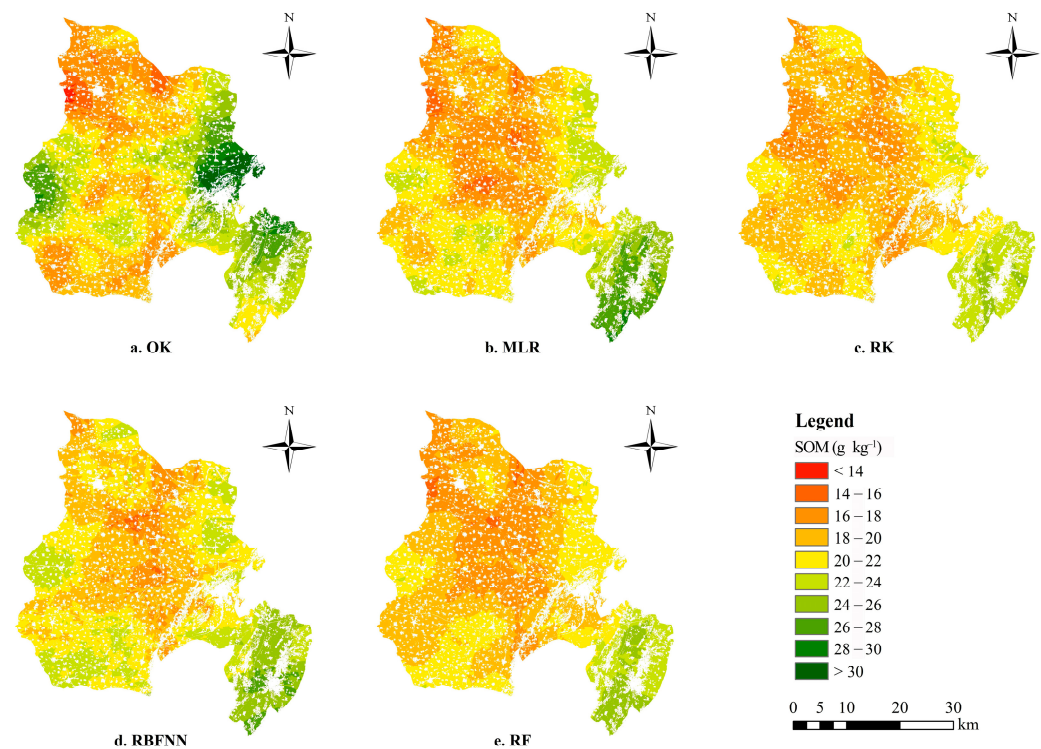


Figure 3. Spatial distribution of predicted SOM content in farmland by OK (a), MLR (b), RK (c), RBFNN (d), and RF (e) models.

4. Discussions

4.1. Relationship between SOM and Environmental Covariates

The spatial distribution of SOM is subjected to various natural and anthropogenic factors, such as soil attributes, climate, topography, vegetation, and human activities [50,51]. By exploring the relationship between SOM and environmental covariates, the accuracy of DSM can be effectively improved [25,43]. In the present study, as shown in Table 4, AN, AK, pH, and MAP are considered the main controlling factors affecting the spatial distribution of SOM. The local dependence diagram of SOM and environmental covariates reflects the specific impact range of AN, AK, pH, and MAP on SOM (Figure 4). This demonstrated that the soil attributes were by far the most influential predictor variables for SOM distribution. The contribution rate of soil AN to SOM prediction exceeds 26.11%, and the AN is positively correlated with the predicted value of SOM (12.6–22.9 g kg⁻¹) in the range of 38–156 mg kg⁻¹ (Figure 4). It is widely known that SOM is an important source of nitrogen in the soil, and the higher the content of organic matter, the more nitrogen transformed into an organic state and accumulated in the soil [52]. The effect of AK on SOM is similar to that of AN, indicating that the increase in available nutrients can notably increase the content of SOM. In this study, AK is positively correlated with the predicted value of SOM (15.7–21.3 g kg⁻¹) in the range of 34–268 mg kg⁻¹ (Figure 4). Soil pH affects the decomposition, mineralization, and colloidal aggregation of SOM [53,54]. In this study, when the pH value is between 5.0–8.7, the predicted value of SOM decreases slightly with the increase in pH; while when the pH exceeds 8.2, the SOM decreases rapidly from 19.8 g kg⁻¹ to 18.3 g kg⁻¹ with the increase in pH value (Figure 4). Grybos et al. [55] reported that under the influence of high soil pH, plant growth may be limited by the decrease in solubility of zinc, iron, and manganese, and the input of crop residues to the soil is limited, resulting in low surface SOM content. In terms of importance, bioclimatic variables are followed by remote sensing data and DEM derivatives. Climate factors such as precipitation

and temperature have been proven to be important factors affecting SOM. Generally, higher precipitation is conducive to plant growth and decelerates the decomposition of organic matter, thereby increasing SOM [33,34]. Consistent with earlier studies [56,57], our study indicated the MAP makes a considerable contribution in modeling SOM, as it explained 13.26% of SOM variations, and positively correlated with SOM ($17.2\text{--}22.1\text{ g kg}^{-1}$) in the range of 730–800 mm (Figure 4).

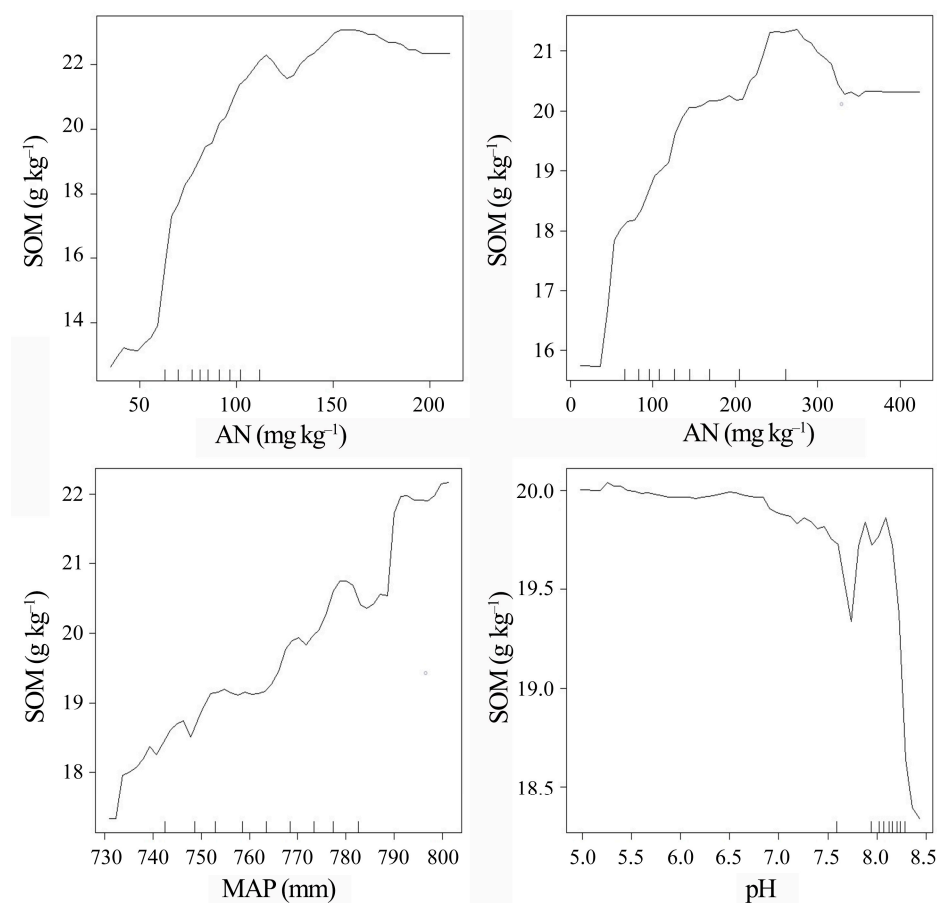


Figure 4. Response of SOM content to the variation of each auxiliary variable. AN: alkali-hydrolyzable nitrogen; AK: available potassium; MAP: mean annual precipitation.

Terrain factors are considered the important factors affecting SOM by regulating the water transportation, substance spatial migration, and the redistribution of solar radiation [30,32]. In comparison to soil attributes and climate factors, the contribution of terrain factors to SOM is not prominent in the current study, which is also demonstrated by former studies [12,58]. This may be owing to the relative single geomorphic type in the study area, with more than 75% of the plain area. Simultaneously, an earlier study has shown that precipitation is the mediating variable for terrain factors such as elevation to affect the spatial distribution of SOM [57]; therefore, precipitation has a greater impact on the prediction of SOM, which reduces the importance of terrain factors in the model to a certain extent. As shown in Table 3, the elevation and slope have an extremely significant positive correlation with SOM, which is mainly because forestland and grassland are mainly distributed in these areas [31]. It is particularly notorious that more abundant litter and less human disturbance are conducive to the accumulation of SOM in these areas [59]. What is more, SOM has a significant positive correlation with RDLS, SCD, and SR, indicating that the comprehensive terrain variables representing the degree of surface erosion exert a positive effect on the spatial distribution of SOM [17].

Remote sensing data provide complete and high-precision surface reflectance data, which can characterize the surface differences of soil attributes by retrieving the corresponding vegetation index [23,38]. In this study, it is found that there is a negative correlation between the ratio of the spectral index and the SOM (Table 3). Among them, Band 2/Band 7, Band 3/Band 7, and Band 4/Band 7 indicate that the short wavelength infrared of Landsat 8 images may play an important role in retrieving the SOM. Previous studies have emphasized that Band 7 has a high sensitivity to soil-available water, and the accumulation of SOM is significantly related to soil-available water [60,61]. In addition, previous studies have shown that SOM has a special spectral reflectance response band in the near-infrared band and visible spectrum [39], while Liu et al. [62] believe that one of the important bands for estimating SOM is around 350–800 nm. Therefore, the reciprocal spectral index combination of Band 2, Band 3, Band 4, and Band 7 can optimize the prediction model of SOM.

4.2. Comparison of Prediction Performance of Different Models

In this study, the RBFNN and RF performed much better than OK, MLR, and RK in the prediction of SOM. In the spatial prediction of SOM, the OK interpolation is based on the principle of spatial autocorrelation; it estimates the attribute value of the non-sampled points according to the structural characteristics of the existing sample points, which does not consider the environmental factors closely related to the change of SOM; and the interpolation accuracy is affected by the sampling quantity and density [15]. Additionally, OK interpolation easily causes a smoothing effect and brings large errors, which is not suitable for exploring areas with complex environmental conditions [42,63]. The MLR method can intuitively show the linear relationship between SOM and the main influencing factors, while cannot reveal the complex relationship of nonlinear interaction between SOM and multiple environmental variables [22,64]. The RK method can not only make full use of neighborhood information for OK interpolation when the residual term has spatial autocorrelation but also effectively establishes a global regression model according to the relationship between SOM and environmental variables [42,45]. Earlier studies have revealed that the RK method significantly weakens the smoothing effect and improves the prediction accuracy compared with OK interpolation [16,17]. The RBFNN network has a simple structure and fast convergence speed, which can effectively overcome the shortcomings of many adjustment parameters and easily fall into local minimum [31]. Even under certain conditions, RBFNN can locally approximate all single-valued continuous functions with any accuracy [46], so it is ideal to describe and simulate the heterogeneity of SOM. Previous studies demonstrated that the RBFNN model integrating environmental variables can better fit the regional distribution of the original data and further reveal the actual spatial variation information of soil attributes [36,47], which is consistent with the conclusion of this study. In this study, K-nearest neighbor analysis is used to determine the expansion constants from different centers, which overcomes the shortage of the same weight of environmental variables in different spatial directions in the traditional model, which describes the local information in detail and effectively improves the prediction, accuracy, and generalization ability [25]. Our study demonstrated that the RF model achieved the highest prediction accuracy for mapping the SOM of farmland in Huang-Huai-Hai Plain, which is consistent with the farmland in southwest China [7], northeast and North Plain China [24], and Nepal [20]. This is owing to the RF having fewer constraints on sample collection and the ability to deal with robust outliers [12,48,64]. Moreover, RF can easily break through the shortcomings of overfitting and the low accuracy of traditional classification models with nonlinear algorithms and has the advantage of explaining most variables with less parameter adjustment [35,42]. In this study, the RF method accurately reveals the nonlinear relationship between SOM and multi-source environmental variables, which fits best with the actual distribution of the study area and does not need to omit the complex action mechanism of environmental variables on SOM due to multicollinearity.

In this study, the terrain, climate, vegetation, primary productivity, spectral, and soil attribute parameters were chosen as conveniently accessible environmental covariates to participate in SOM modeling. The sources and precision of the auxiliary variable data gathered in this study vary, however; for example, there is a DEM resolution of 30m and a MAT, MAP, and NPP of 1 km. Grid resampling may alter the accuracy of auxiliary variable data while unifying spatial resolution. Moreover, the soil attribute grid data is created by interpolating the soil sample data using ordinary Kriging, which may cause error transmission and superposition and, as a result, affect prediction accuracy to some extent. Furthermore, SOM is tightly linked to human activities in dryland agroecosystems, and covariates characterizing human activities such as tillage systems and fertilization methods were not included in the model predictions due to limited data acquisition. The practice has proven that agricultural activities such as rotation, irrigation, and fertilization significantly impact SOM [3,7,65]. Therefore, finding more auxiliary variables with a strong correlation with the SOM and alternative factors that can represent human activities as model inputs will be among the important ways in which to improve the accuracy of SOM prediction.

5. Conclusions

In the present study, multi-source environmental covariates are selected to map the spatial distribution of SOM in a typical dryland agroecosystem via OK, MLR, RK, RBFNN, and RF models. The results reveal that the SOM content is closely correlated with soil attributes, terrain factors, and climate factors. Furthermore, AN, AK, MAP, and pH are the main controlling factors affecting the spatial distribution of SOM, which jointly contribute 68.9% of the variation of SOM. The RF model achieved higher accuracy in predicting soil SOM than other models, with higher R^2 (0.48) and lower MAE (2.38 g kg^{-1}), MRE (12.99%), and RMSE (3.14 g kg^{-1}). Moreover, the predicted map revealed that farmland distributed in the center and northwest of the study area had a lower SOM, while farmland distributed in the southeast had a higher SOM. Collectively, our study confirms that machine learning-based models have some merit in predicting SOM in dryland agroecosystems and provides a new insight into mapping SOM content and implementing the sustainable agricultural management of farmland soils.

Author Contributions: Conceptualization, X.X.; Methodology, H.J.; Writing—original draft, H.J. and X.X.; Supervision, L.P., Z.J. and F.X.; Project administration, X.X.; Funding acquisition, L.P. and X.X. All authors have read and agreed to the published version of the manuscript.

Funding: This research was funded by the National Natural Science Foundation of China (42101068, 42171245, 41701618) and the Natural Science Foundation of Zhejiang Province (LQ21D010007).

Data Availability Statement: Not applicable.

Conflicts of Interest: The authors declare no conflict of interest.

References

1. Reeves, D.W. The role of soil organic matter in maintaining soil quality in continuous cropping systems. *Soil Tillage Res.* **1997**, *43*, 131–167. [[CrossRef](#)]
2. Xie, X.F.; Pu, L.J.; Zhu, M.; Wu, T.; Wang, X.H. Effect of long-term reclamation on soil quality in agricultural reclaimed coastal saline soil, eastern China. *J. Soil Sediments* **2020**, *20*, 3909–3920. [[CrossRef](#)]
3. Xie, X.F.; Pu, L.J.; Zhu, M.; Meadows, M.; Sun, L.C.; Wu, T.; Bu, X.G.; Xu, Y. Differential effects of various reclamation treatments on soil characteristics: An experimental study of newly reclaimed tidal mudflats on the east China coast. *Sci. Total Environ.* **2021**, *768*, 144996. [[CrossRef](#)] [[PubMed](#)]
4. Adhikari, K.; Hartemink, A.E. Linking soils to ecosystem services—A global review. *Geoderma* **2016**, *262*, 101–111. [[CrossRef](#)]
5. Bünemann, E.K.; Bongiorno, G.; Bai, Z.; Creamer, R.E.; De Deyn, G.; De Goede, R.; Fleskens, L.; Geissen, V.; Kuyper, T.W.; Mäder, P.; et al. Soil quality—A critical review. *Soil Biol. Biochem.* **2018**, *120*, 105–125. [[CrossRef](#)]
6. Hoffland, E.; Kuyper, T.W.; Comans, R.; Creamer, R.E. Eco-functionality of organic matter in soils. *Plant Soil* **2020**, *455*, 1–22. [[CrossRef](#)]

7. Hu, B.F.; Ni, H.J.; Xie, M.D.; Li, H.Y.; Wen, Y.L.; Chen, S.C.; Zhou, Y.; Teng, H.F.; Bourennane, H.; Shi, Z. Mapping soil organic matter and identifying potential controls in the farmland of Southern China: Integration of multi-source data, machine learning and geostatistics. *Land Degrad. Dev.* **2023**, *early view*. [[CrossRef](#)]
8. Nuralykyzy, B.; Nurzhan, A.; Li, N.; Huang, Q.; Zhu, Z.L.; An, S.S. Influence of land use types on soil carbon fractions in the Qaidam Basin of the Qinghai-Tibet Plateau. *Catena* **2023**, *231*, 107273. [[CrossRef](#)]
9. Poepflau, C.; Prietz, R.; Don, A. Plot-scale variability of organic carbon in temperate agricultural soils—Implications for soil monitoring. *J. Plant Nutr. Soil Sci.* **2022**, *185*, 403–416. [[CrossRef](#)]
10. Bahri, H.; Raclot, D.; Barbouchi, M.; Lagacherie, P.; Annabi, M. Mapping soil organic carbon stocks in Tunisian topsoils. *Geoderma Reg.* **2022**, *30*, e00561. [[CrossRef](#)]
11. Minasny, B.; McBratney, A.B. Methodologies for Global Soil Mapping. In *Digital Soil Mapping*; Springer: Dordrecht, The Netherlands, 2010; pp. 429–436.
12. Guo, P.T.; Li, M.F.; Luo, W.; Tang, Q.F.; Liu, Z.W.; Lin, Z.M. Digital mapping of soil organic matter for rubber plantation at regional scale: An application of random forest plus residuals kriging approach. *Geoderma* **2015**, *237–238*, 49–59. [[CrossRef](#)]
13. Coelho, F.F.; Giasson, E.; Campos, A.R.; Silva, R.G.P.O.; Costa, J.J.F. Geographic object-based image analysis and artificial neural networks for digital soil mapping. *Catena* **2021**, *206*, 105568. [[CrossRef](#)]
14. Chaplot, V.; Walter, C.; Curmi, P. Improving soil hydromorphy prediction according to DEM resolution and available pedological data. *Geoderma* **2000**, *97*, 405–422. [[CrossRef](#)]
15. Xie, X.F.; Pu, L.J.; Zhu, M.; Wu, T.; Xu, Y. Spatio-temporal variability of soil salinity and sodicity in agricultural reclaimed coastal wetlands, Eastern China. *Arch. Agron. Soil Sci.* **2020**, *66*, 1639–1650. [[CrossRef](#)]
16. Andrew, S.; Ganesh, P.; Keith, S. Evaluating regression-kriging for mid-infrared spectroscopy prediction of soil properties in western Kenya. *Geoderma Reg.* **2017**, *10*, 39–47.
17. Owusu, S.; Yigini, Y.; Olmedo, G.F.; Omuto, C.T. Spatial prediction of soil organic carbon stocks in Ghana using legacy data. *Geoderma* **2020**, *360*, 114008. [[CrossRef](#)]
18. Grimm, R.; Behrens, T.; Mrker, M.; Elsenbeer, H. Soil organic carbon concentrations and stocks on Barro Colorado Island—Digital soil mapping using Random Forests analysis. *Geoderma* **2008**, *146*, 102–113. [[CrossRef](#)]
19. Li, Q.Q.; Yue, T.X.; Wang, C.Q.; Zhang, W.J.; Yu, Y.; Li, B.; Yang, J.; Bai, G.C. Spatially distributed modeling of soil organic matter across China: An application of artificial neural network approach. *Catena* **2013**, *104*, 210–218. [[CrossRef](#)]
20. Lamichhane, S.; Adhikari, K.; Kumar, L. National soil organic carbon map of agricultural lands in Nepal. *Geoderma Reg.* **2022**, *30*, e00568. [[CrossRef](#)]
21. Zhang, P.P.; Wang, Y.Q.; Sun, H.; Qi, L.J.; Liu, H.; Wang, Z. Spatial variation and distribution of soil organic carbon in an urban ecosystem from high-density sampling. *Catena* **2021**, *204*, 105364. [[CrossRef](#)]
22. Xie, X.F.; Wu, T.; Zhu, M.; Jiang, G.J.; Xu, Y.; Wang, X.H.; Pu, L.J. Comparison of random forest and multiple linear regression models for estimation of soil extracellular enzyme activities in agricultural reclaimed coastal saline land. *Ecol. Indic.* **2021**, *120*, 106925. [[CrossRef](#)]
23. Zhou, T.; Geng, Y.J.; Ji, C.; Xu, X.R.; Wang, H.; Pan, J.J.; Bumberger, J.; Haase, D.; Lausch, A. Prediction of soil organic carbon and the C:N ratio on a national scale using machine learning and satellite data: A comparison between Sentinel-2, Sentinel-3 and Landsat-8 images. *Sci. Total Environ.* **2021**, *755*, 142661. [[CrossRef](#)]
24. Zhang, X.; Xue, J.; Chen, S.; Wang, N.; Shi, Z.; Huang, Y.; Zhuo, Z. Digital Mapping of Soil Organic Carbon with Machine Learning in Dryland of Northeast and North Plain China. *Remote Sens.* **2022**, *14*, 2504. [[CrossRef](#)]
25. Zeraatpisheh, M.; Garosi, Y.; Owliaie, H.R.; Ayoubi, S.; Taghizadeh-Mehrjardi, R.; Scholten, T.; Xu, M. Improving the spatial prediction of soil organic carbon using environmental covariates selection: A comparison of a group of environmental covariates. *Catena* **2022**, *208*, 105723. [[CrossRef](#)]
26. Wiesmeier, M.; Barthold, F.; Blank, B.; Kögel-Knabner, I. Digital mapping of soil organic matter stocks using random forest modeling in a semi-arid steppe ecosystem. *Plant Soil* **2011**, *340*, 7–24. [[CrossRef](#)]
27. Chagas, C.; Junior, W.; Bhering, S.B.; Filho, B.C. Spatial prediction of soil surface texture in a semiarid region using random forest and multiple linear regressions. *Catena* **2016**, *139*, 232–240. [[CrossRef](#)]
28. Gibson, A.J.; Hancock, G.R.; Bretreger, D.; Cox, T.; Hughes, J.; Kunkel, V. Assessing digital elevation model resolution for soil organic carbon prediction. *Geoderma* **2021**, *398*, 115106. [[CrossRef](#)]
29. Lu, R.K. *Chemical Analysis of Agricultural Soils*; China Agricultural Science and Technology Press: Beijing, China, 1999.
30. Veronesi, F.; Schillaci, C. Comparison between geostatistical and machine learning models as predictors of topsoil organic carbon with a focus on local uncertainty estimation. *Ecol. Indic.* **2019**, *101*, 1032–1044. [[CrossRef](#)]
31. Wang, C.; Cui, Y.; Ma, Z.; Guo, Y.; Zhang, M. Simulating spatial variation of soil carbon content in the Yellow River Delta: Comparative analysis of two artificial neural network models. *Wetlands* **2020**, *40*, 223–233. [[CrossRef](#)]
32. Mahmoudzadeh, H.; Matinfar, H.R.; Taghizadeh-Mehrjardi, R.; Kerry, R. Spatial prediction of soil organic carbon using machine learning techniques in western Iran. *Geoderma Reg.* **2020**, *21*, e00260. [[CrossRef](#)]
33. Zhang, K.; Dang, H.; Zhang, Q.; Cheng, X. Soil carbon dynamics following land-use change varied with temperature and precipitation gradients: Evidence from stable isotopes. *Glob. Chang. Biol.* **2015**, *21*, 2762–2772. [[CrossRef](#)] [[PubMed](#)]
34. Liu, E.; Liu, J.; Yu, K.; Wang, Y.; He, P. A hybrid model for predicting spatial distribution of soil organic matter in a bamboo forest based on general regression neural network and iterative algorithm. *J. For. Res.* **2020**, *31*, 1673–1680. [[CrossRef](#)]

35. Pouladi, N.; Møller, A.B.; Tabatabai, S.; Greve, M.H. Mapping soil organic matter contents at field level with Cubist, Random Forest and kriging. *Geoderma* **2019**, *342*, 85–92. [[CrossRef](#)]
36. Ye, Y.; Jiang, Y.; Kuang, L.; Han, Y.; Guo, X. Predicting spatial distribution of soil organic carbon and total nitrogen in a typical human impacted area. *Geocarto Int.* **2022**, *37*, 4465–4482. [[CrossRef](#)]
37. Zhang, X.; Jia, J.; Chen, L.; Chu, H.; He, J.S.; Zhang, Y.J.; Feng, X. Aridity and NPP constrain contribution of microbial necromass to soil organic carbon in the Qinghai-Tibet alpine grasslands. *Soil Biol. Biochem.* **2021**, *156*, 108213. [[CrossRef](#)]
38. Junior, W.; Lagacherie, P.; Chagas, C.; Filho, B.C.; Bhering, S.B. A regional-scale assessment of digital mapping of soil attributes in a tropical hillslope environment. *Geoderma* **2014**, *232–234*, 479–486. [[CrossRef](#)]
39. Zheng, G.; Ryu, D.; Jiao, C.; Hong, C. Estimation of organic matter content in coastal soil using reflectance spectroscopy. *Pedosphere* **2016**, *26*, 130–136. [[CrossRef](#)]
40. Jin, X.; Song, K.; Du, J.; Liu, H.; Wen, Z. Comparison of different satellite bands and vegetation indices for estimation of soil organic matter based on simulated spectral configuration. *Agric. For. Meteorol.* **2017**, *244–245*, 57–71. [[CrossRef](#)]
41. Wei, F.; Liu, J.; Xia, L.; Xu, Z.; Long, X. Spatial prediction method of farmland soil organic matter in Weibei Dryland of Shaanxi Province. *Environ. Sci.* **2022**, *43*, 1097–1107.
42. Boubehziz, S.; Khanchoul, K.; Benslama, A.; Marchetti, A.; Francaviglia, R.; Piccini, C. Predictive mapping of soil organic carbon in Northeast Algeria. *Catena* **2020**, *190*, 104539. [[CrossRef](#)]
43. Zhang, M.W.; Liu, H.J.; Zhang, M.N.; Yan, H.X.; Jin, Y.L.; Han, Y.; Tang, H.T.; Zhang, X.H.; Zhang, X.L. Mapping soil organic matter and analyzing the prediction accuracy of typical cropland soil types on the Northern Songnen Plain. *Remote Sens.* **2021**, *13*, 5162. [[CrossRef](#)]
44. McBratney, A.B.; Odeh, I.O.A.; Bishop, T.F.A.; Dunbar, M.S.; Shatar, T.M. An overview of pedometric techniques for use in soil survey. *Geoderma* **2000**, *97*, 293–327. [[CrossRef](#)]
45. Li, Y. Can the spatial prediction of soil organic matter contents at various sampling scales be improved by using regression kriging with auxiliary information. *Geoderma* **2010**, *159*, 63–75. [[CrossRef](#)]
46. Li, Q.Q.; Zhang, X.; Wang, C.Q.; Li, B.; Gao, X.S.; Yuan, D.G.; Luo, Y.L. Spatial prediction of soil nutrient in a hilly area using artificial neural network model combined with kriging. *Arch. Agron. Soil Sci.* **2016**, *62*, 1541–1553. [[CrossRef](#)]
47. Sabour, M.R.; Mofakhari, S.; Movahed, A. Application of radial basis function neural network to predict soil sorption partition coefficient using topological descriptors. *Chemosphere* **2017**, *168*, 877–884. [[CrossRef](#)] [[PubMed](#)]
48. Breiman, L. Random forests. *Mach. Learn.* **2001**, *45*, 5–32. [[CrossRef](#)]
49. National Soil Survey Office. *Soil Survey Technique in China*; Agricultural Press: Beijing, China, 1992.
50. Zhao, M.S.; Zhang, G.L.; Wu, Y.J.; Li, D.C.; Zhao, Y.G. Driving forces of soil organic matter change in Jiangsu province of China. *Soil Use Manag.* **2015**, *31*, 440–449. [[CrossRef](#)]
51. Du, Z.; Gao, B.; Ou, C.; Du, Z.; Zhu, D. A quantitative analysis of factors influencing organic matter concentration in the topsoil of black soil in Northeast China based on spatial heterogeneous patterns. *Int. J. Geo-Inf.* **2021**, *10*, 348. [[CrossRef](#)]
52. Huang, B.; Sun, W.X.; Zhao, Y.C.; Zhu, J.; Yao, R.J.; Zou, Z.; Ding, F.; Su, J.P. Temporal and spatial variability of soil organic matter and total nitrogen in an agricultural ecosystem as affected by farming practices. *Geoderma* **2007**, *139*, 336–345. [[CrossRef](#)]
53. Motavalli, P.P.; Palm, C.A.; Parton, W.J.; Elliott, E.T.; Frey, S.D. Soil pH and organic C dynamics in tropical forest soils: Evidence from laboratory and simulation studies. *Soil Biol. Biochem.* **1995**, *27*, 1589–1599. [[CrossRef](#)]
54. Tian, Y.; Takamashi, K.; Toda, H.; Haibara, K.; Ding, F. pH and substrate regulation of nitrogen and carbon dynamics in forest soils in a karst region of the upper Yangtze River Basin, China. *J. For. Res.* **2013**, *18*, 228–237. [[CrossRef](#)]
55. Grybos, M.; Davranche, M.; Gruau, G.; Petitjean, P.; Pédrot, M. Increasing pH drives organic matter solubilization from wetland soils under reducing conditions. *Geoderma* **2009**, *154*, 13–19. [[CrossRef](#)]
56. Feyissa, A.; Raza, S.T.; Cheng, X. Soil carbon stabilization and potential stabilizing mechanisms along elevational gradients in alpine forest and grassland ecosystems of Southwest China. *Catena* **2023**, *229*, 107210. [[CrossRef](#)]
57. Osland, M.J.; Gabler, C.A.; Grace, J.B.; Day, R.H.; McCoy, M.; McLeod, J.L.; From, A.S.; Enwright, N.M.; Feher, L.C.; Stagg, C.; et al. Climate and plant controls on soil organic matter in coastal wetlands. *Glob. Chang. Biol.* **2018**, *24*, 5361–5379. [[CrossRef](#)] [[PubMed](#)]
58. Zhou, Y.; Biswas, A.; Ma, Z.Q.; Lu, Y.L.; Chen, Q.X.; Shi, Z. Revealing the scale-specific controls of soil organic matter at largescale in northeast and North China plain. *Geoderma* **2016**, *271*, 71–79. [[CrossRef](#)]
59. Bull, I.D.; Bergen, P.F.; Bol, R.; Brown, S.; Gledhill, A.R.; Gray, A.J.; Harkness, D.D.; Woodbury, S.E.; Evershed, R.P. Estimating the contribution of spartina anglica biomass to salt-marsh sediments using compound specific stable carbon isotope measurements. *Org. Geochem.* **1999**, *30*, 477–483. [[CrossRef](#)]
60. Dematte, J.; Fiorio, P.R.; Ben-Dor, E. Estimation of soil properties by orbital and laboratory reflectance means and its relation with soil classification. *Open Remote Sen. J.* **2009**, *2*, 12–23. [[CrossRef](#)]
61. Liao, K.H.; Xu, S.H.; Wu, J.C.; Zhu, Q. Spatial estimation of surface soil texture using remote sensing data. *Soil Sci. Plant Nutr.* **2013**, *59*, 488–500. [[CrossRef](#)]
62. Liu, Y.; Jiang, Q.; Fei, T.; Wang, J.; Shi, T.; Kai, G.; Li, X.; Chen, Y. Transferability of a visible and near-infrared model for soil organic matter estimation in riparian landscapes. *Remote Sens.* **2014**, *6*, 4305–4322. [[CrossRef](#)]
63. Tan, Q.; Geng, J.; Fang, H.; Li, Y.; Guo, Y. Exploring the impacts of data source, model types and spatial scales on the soil organic carbon prediction: A case study in the red soil hilly region of Southern China. *Remote Sens.* **2022**, *14*, 5151. [[CrossRef](#)]

64. Ceddia, M.B.; Gomes, A.S.; Vasques, G.M.; Pinheiro, É.F.M. Soil Carbon Stock and Particle Size Fractions in the Central Amazon Predicted from Remotely Sensed Relief, Multispectral and Radar Data. *Remote Sens.* **2017**, *9*, 124. [[CrossRef](#)]
65. Li, Z.; Xu, X.; Pan, G.; Smith, P.; Cheng, K. Irrigation regime affected soc content rather than plow layer thickness of rice paddies: A county level survey from a river basin in lower Yangtze valley, China. *Agric. Water Manag.* **2016**, *172*, 31–39. [[CrossRef](#)]

Disclaimer/Publisher’s Note: The statements, opinions and data contained in all publications are solely those of the individual author(s) and contributor(s) and not of MDPI and/or the editor(s). MDPI and/or the editor(s) disclaim responsibility for any injury to people or property resulting from any ideas, methods, instructions or products referred to in the content.